Magnetic Resonance Imaging, Vol. 17, No. 3, pp. 349–354, 1999

Printed in the USA.
0730-725X/99 $–see front matter

ELSEVIER

PII S0730-725X(98)00171-4

● *Original Contribution*

# CORRELATION OF REGIONAL CEREBRAL BLOOD FLOW FROM PERFUSION MRI AND SPECT IN NORMAL SUBJECTS

THOMAS ERNST,*† LINDA CHANG,† LAURENT ITTI,† AND OLIVER SPECK*

Departments of *Radiology and †Neurology, Harbor UCLA Medical Center, Torrance, CA, USA

**The objective of this study was to determine the relationship in regional cerebral blood flow (rCBF) as measured with perfusion magnetic resonance imaging (pMRI) and single photon emission computer tomography (SPECT). rCBF was determined in 26 healthy subjects with pMRI and SPECT. After co-registration of pMRI with SPECT, rCBF was determined in 10 brain regions relative to the whole slice value. pMRI was evaluated with and without elimination of large vessels. rCBF from pMRI correlates significantly with rCBF from SPECT ($r = 0.69$ with and $r = 0.59$ without elimination of large vessels; $p < 0.0001$ for both). Elimination of large vessels reduced the interindividual variance of the pMRI measurements in most regions. rCBF from pMRI shows good correlation with rCBF from SPECT. Because pMRI is sensitive to flow in large vessels while SPECT is not, elimination of large vessels in pMRI reduces the interindividual variability of pMRI and improves the correlation between the two methods. pMRI is a reliable noninvasive method for rCBF measurements.** **© 1999 Elsevier Science Inc.**

*Keywords:* **Regional cerebral blood flow; Perfusion; SPECT; Normal subjects.**

## INTRODUCTION

Brain perfusion is an important physiological parameter that is closely linked to cerebral metabolism and brain function. Regional cerebral blood flow (rCBF) and volume (rCBV) have been shown to be increased during brain activation and decreased with many neurologic diseases. For more than a decade, two nuclear medicine techniques, positron emission tomography (PET) and single photon emission computed tomography (SPECT), have been used to measure cerebral perfusion in vivo.[1–3] More recently, a new MRI based technique, perfusion MRI or pMRI, has been introduced to measure rCBV and rCBF.[4–7] Perfusion MRI is based on fast dynamic MR imaging during a bolus injection of a gadolinium contrast agent. The advantages of pMRI over PET and SPECT are significant: the MR contrast agent is not radioactive and is relatively inexpensive compared to PET and SPECT tracers. Furthermore, MRI is already performed in many patients, and the additional scan time for the perfusion measurement is less than 2 min.

Although the utility of pMRI in various neurologic diseases is under investigation,[8–11] pMRI is still mainly a research tool which has to prove its clinical usefulness. Little is known about the relationship between cerebral perfusion as measured with SPECT and as measured with pMRI. One of the main differences between the two methods is that pMRI (using $T_2$*-dependent techniques) is sensitive to the presence of larger blood vessels, whereas PET or SPECT do not measure intravascular blood. Therefore, well-known interindividual variations in the cerebral vasculature may lead to increased variability and systematic errors in pMRI measurements of rCBF not present in PET or SPECT. It is the aim of this paper to investigate the effect of the differing methodologies in SPECT and pMRI on quantitative measures of rCBF. Furthermore, we will determine whether elimination of large vessels (ELV), by image-processing, reduces the interindividual variances of pMRI measurements and improves the correlation between pMRI and SPECT.

## MATERIALS AND METHODS

### *Subjects*

Perfusion MRI and SPECT were performed in 26 normal healthy subjects between ages 22 and 85 years

RECEIVED 3/25/98; ACCEPTED 8/8/98.

Address correspondence to Dr. Thomas Ernst, Harbor-UCLA Medical Center, Department of Radiology, 1000 W. Carson Street, N-11, Torrance, CA 90502. E-mail: ernst@afp76.humc.edu

(12 female, 14 male). None of the subjects was on any medications, or had any previous neurologic illnesses, cerebrovascular diseases, hypertension, or diabetes. Structural MRI was normal in all subjects studied. Verbal and written informed consent was obtained from all subjects prior to the first scan. The protocol was approved by the Institutional Review Board at Harbor-UCLA REI.

*Structural MRI*

All MR scans were performed on a clinical 1.5 T GE scanner using a standard quadrature head coil. MRI began with a sagittal $T_1$-weighted localizer [TE/TR 11/500, 4-mm slice thickness, 1-mm gap, 24 cm field-of-view (FOV)], followed by a coronal fast double spin echo sequence (TE1/TE2/TR 17/102/4000, 5-mm slice thickness, no gap, 24 cm FOV). Finally, an axial fast inversion recovery (IR) scan was performed, which yielded excellent contrast between white matter, gray matter and CSF (TE/TI/TR 32/120/4000, 3.5-mm slice thickness, no gap, 24 cm FOV). This fast IR scan was used for co-registration with pMRI and SPECT, and for manual drawing of anatomic regions (see below).

*Perfusion MRI*

The perfusion MRI study was performed on a single axial slice, which was always chosen by the same investigator (L.C.). The position of the perfusion scan was selected to coincide with one of the slices of the IR scan (see Fig. 1). pMRI was performed on an 8 mm slice using a gradient echo sequence with an echo time of 19 ms and a flip angle of 10°. A rectangular field of view of 34 × 17 cm (read × phase direction) was used. In the phase dimension, the 64 projections acquired (with a nominal resolution of 2.6 mm) were interpolated into a 128 × 128 image with an in-plane resolution of 1.3 mm. With a TR of 38 ms, the scan time per image was 2.5 s. This image was acquired sequentially 40 times, yielding a total scan time of about 1:40 min. Perfusion MRI was performed with the subjects' heads in the dimly lit MRI scanner; no visually salient features were present during the scan.

Twenty mL of the gadolinium contrast agent Prohance (Squibb, Princeton, NJ) was manually injected as an intravenous (i.v.) bolus after the first 12 MR images were acquired as baseline scans. The first noticeable change in the MR signal occurred approximately 10 s after the injection (at image #16), and the maximum signal change was observed about 20 s after injection (at image #20). The signal intensity returned to baseline by scan #25, and the last 13 scans served as post-injection baseline.

The 40 sequential images were transferred to a DEC Alpha workstation (Digital Equipment Corporation, Nashua, NH). To extract the regional blood flow for each MRI pixel, a program written in IDL (Research Systems, Boulder, CO) and the C-language was developed in our laboratory. The algorithm for extracting the rCBF value from the 40 sequential MR images was based on the fact that the MR signal is exponentially related to the relaxation time $T_2^*$ which, in turn, was assumed to be inversely proportional to the concentration of the contrast agent.[12] For each pixel, the measured time course of the MRI signal was fitted to a modified gamma function,[13] using Powell's algorithm. The fit yielded the mean transit time (MTT) and the area under the curve (which is proportional to the regional cerebral blood volume rCBV). From these two quantities, rCBF was calculated using the equation: rCBF = rCBV/MTT. The resulting image was displayed as an rCBF map (see Fig. 1) using a color scale.

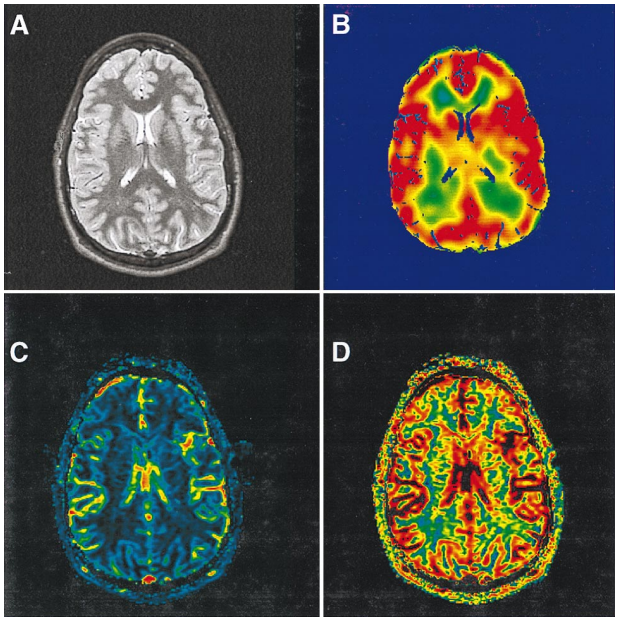


Fig. 1. Representative images of co-registered MRI (A), SPECT (B), and perfusion MRI without (C) and with (D) elimination of large vessels from a healthy volunteer. The slice shown is located at the level of the basal ganglia, internal capsule and thalamus. The color scale used to display perfusion ranges from blue (lowest) through yellow and orange to red (highest).

*SPECT*

All subjects were evaluated with Technetium-99 HMPAO[14] on a brain dedicated SPECT scanner (Headtome II, Shimadzu, Kyoto, Japan). Each subject received 1100 MBq of $^{99m}$Tc-HMPAO i.v. in a darkened room with their eyes closed. The SPECT scanning started 30–60 min after injection of the HMPAO to clear soft-tissue and muscle background activity of the face and neck.

The subjects were scanned for about 30 min. The resolution of the SPECT images was approximately 8 mm (in-plane) and 16 mm slice thickness. The partial volume of CSF was determined from the high-resolution IR scan and was used to correct the SPECT images for CSF content.[15]

*Coregistration of SPECT and MRI*

To correlate rCBF measured with the two methods, SPECT and perfusion MR images were co-registered using a customized co-registration software package developed in our laboratory.[16] The co-registration program was based on a surface matching algorithm. First, the brain surfaces from the SPECT scan and from the axial IR scan were extracted automatically. Next, the two data sets were aligned using iterative anisotropic chamfer matching of the two surfaces. The precision of this procedure was better than 1 mm.[16] The MR images were used to determine the partial volume of CSF in each SPECT voxel, and to correct the blood flow values correspondingly (assuming that there is no tracer uptake in the CSF). The SPECT images were resliced to be parallel to the single slice used for the perfusion MRI (Fig. 1). The co-registration software allowed for quantitative analysis of any number of manually drawn regions of interest on the aligned SPECT and perfusion images. All regions of interest were drawn on the high-resolution axial inversion-recovery images, and were applied simultaneously to the pMRI and SPECT blood flow maps. Figure 2 shows the regions that were analyzed (if visible on the IR images): 1) frontal (typical area 10 $cm^2$); 2) temporal (15 $cm^2$); 3) parietal (4 $cm^2$); and 4) visual cortex (4 $cm^2$); 5) caudate (1.5 $cm^2$); 6) putamen (2.5 $cm^2$); 7) globus pallidus (1.5 $cm^2$); 8) thalamus (3 $cm^2$); and 9) frontal (6 $cm^2$) and 10) temporo-parietal white matter (10 $cm^2$). The respective values from the left and right hemispheres were averaged.

*Elimination of Large Vessels (ELV)*

Because gradient-echo images are sensitive to the presence of large vessels, while perfusion measures from SPECT do not account for them, the perfusion MR images were evaluated with and without elimination of large vessels. To determine rCBF corrected for large vessels, all pixels with an rCBF value above a certain threshold were defined to contain a large vessel, and were excluded from the calculation of the rCBF in the regions analyzed. The threshold for this procedure was defined as 2.5 times the median of all rCBF values in the corresponding rCBF map (excluding pixels outside of the brain). A typical histogram is shown in Fig. 3.

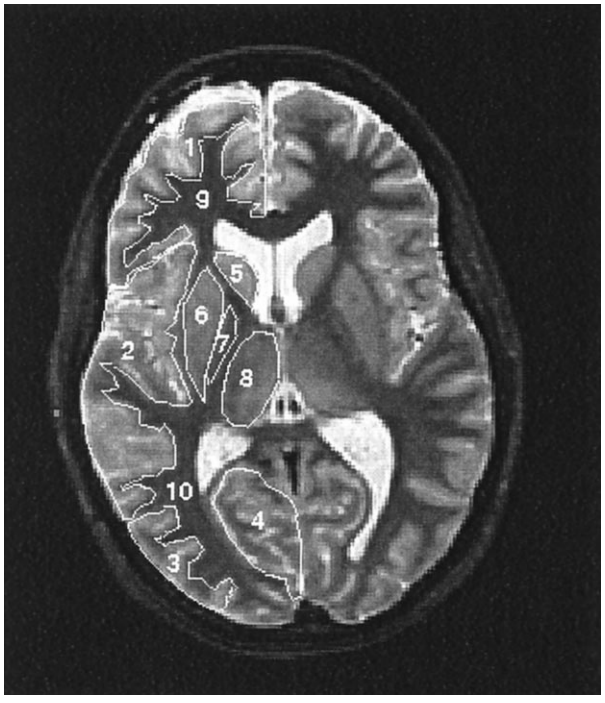


Fig. 2. Regions of interest used for the analysis of cerebral perfusion. The following regions were evaluated: 1) frontal, 2) temporal, 3) parietal, and 4) visual cortex, 5) caudate, 6) putamen, 7) globus pallidus, 8) thalamus, and 9) frontal and 10) temporo-parietal white matter.

*Statistical Analysis*

For each method, the rCBF value of each region was expressed relative to the corresponding average value of the whole slice. Linear regression analyses between these

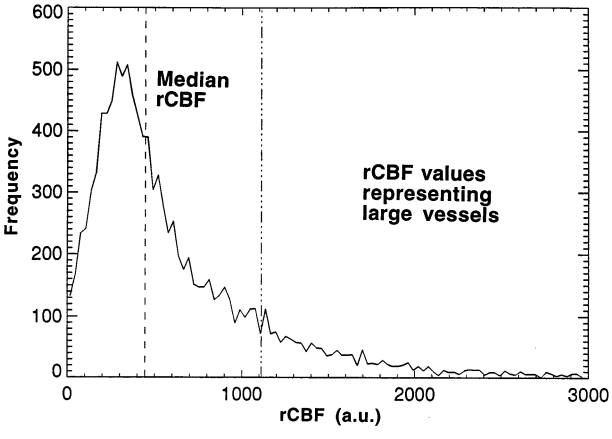


Fig. 3. Typical histogram of rCBF values. To eliminate larger vessels, the median rCBF value is calculated from the histogram, and all pixels with a value greater than 2.5 times the median are excluded from further analysis.

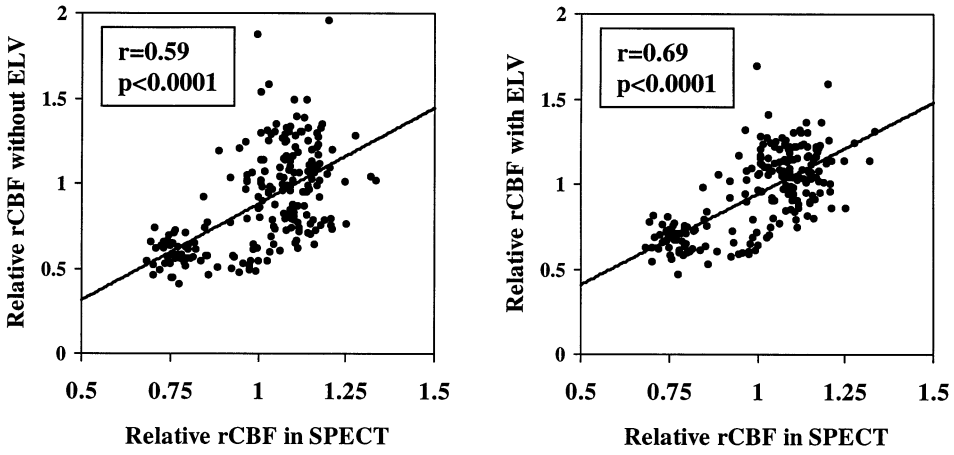


Fig. 4. Regression of rCBF from SPECT with rCBF from pMRI (left) without ELV and (right) with ELV using all volunteers and all regions ($n = 217$). Elimination of large vessels in pMRI considerably improves the correlation with SPECT.

relative perfusion values were performed; SPECT was used as the independent measure. To determine whether differences in the variances of the pMRI data with and without ELV were statistically significant within a given region, a non-parametric paired sign-test was used to compare the squared individual relative deviations from the mean with and without ELV. The statistical analyses were performed on a Macintosh computer using the StatView program (Abacus, Berkeley, CA). All statistical tests were two-tailed; *p*-values smaller than 0.05 were considered statistically significant, whereas *p*-values between 0.05 and 0.1 were defined as a trend.

## RESULTS

Figure 4 shows a scatter plot of rCBF from pMRI vs. rCBF from SPECT, using the individual data points from all regions and all subjects ($n = 217$). The regression coefficients were 0.59 without ELV and 0.69 with ELV ($p < 0.0001$ for both cases); the slopes of the regression curves were 1.13 without and 1.07 with ELV. However, the regression coefficients were considerably smaller when only gray matter regions were considered ($r = 0.25$, $p = 0.001$ without ELV; $r = 0.35$, $p < 0.0001$ with ELV; $n = 164$). In individual regions, significant correlations between SPECT and pMRI were observed in the parietal gray matter ($r = 0.42$, $p = 0.04$ with ELV; $r = 0.53$, $p = 0.007$ without ELV) and in the globus pallidus ($r = 0.65$, $p = 0.01$ with ELV).

Table 1 shows the average relative rCBF from pMRI and SPECT in the 10 regions analyzed. White matter had

Table 1. Average values ± standard deviations (in %) for relative rCBF from pMRI without and with ELV, and from SPECT in 10 brain regions

| | pMRI without ELV | pMRI with ELV | *P*-value (difference in relative variance) | SPECT |
|---|---|---|---|---|
| Frontal gray matter | 1.09 ± 15% | 1.08 ± 9% | <0.0001 | 1.06 ± 9% |
| Temporal gray matter | 1.30 ± 11% | 1.23 ± 7% | 0.03 | 1.09 ± 4% |
| Parietal matter | 1.06 ± 14%* | 1.11 ± 9%† | (0.1) | 1.04 ± 6% |
| Visual cortex | 1.11 ± 12% | 1.17 ± 7% | 0.004 | 1.16 ± 5% |
| Caudate | 0.88 ± 19% | 1.02 ± 15% | 0.03 | 1.12 ± 7% |
| Putamen | 0.75 ± 12% | 0.90 ± 11% | 0.04 | 1.09 ± 5% |
| Globus pallidus | 0.55 ± 9% | 0.65 ± 11%† | NS | 0.98 ± 4% |
| Thalamus | 0.98 ± 29% | 1.07 ± 19% | NS | 1.14 ± 6% |
| Frontal white matter | 0.59 ± 15% | 0.68 ± 13% | NS | 0.81 ± 6% |
| Temporo–parietal white matter | 0.58 ± 12% | 0.67 ± 9% | (0.08) | 0.75 ± 5% |

The p-values indicate the statistical significance of differences in the (relative) variance of pMRI with and without ELV.
* $p \leq 0.05$ for correlation between pMRI and SPECT.
† $p \leq 0.01$ for correlation between pMRI and SPECT.

low blood flow with both techniques. SPECT exhibited relatively homogeneous blood flow in cortical and deep gray matter (range 0.98–1.16). In contrast, rCBF in pMRI spanned a larger range, although less with ELV (range 0.65–1.23) than without ELV (range 0.55–1.30). Furthermore, ELV statistically significantly reduced the interindividual standard deviations in most of the regions analyzed; in particular, the standard deviations of rCBF in all four cortical regions was below 10% after ELV (see Table 1 for the *p*-values).

## DISCUSSION

*Mechanisms*

It is the aim of this study to investigate the effect of methodological differences between pMRI and SPECT on rCBF measurements. Because SPECT and pMRI are based on two different mechanisms, the relationship between the two methods is far from obvious. SPECT relies on the diffusion of a lipophilic radioactive tracer (HMPAO in our study) across the blood–brain barrier, and its chemical conversion into a hydrophilic compound that is trapped within the brain parenchyma. This mechanism yields a good estimate of rCBF at the capillary level.[14] The intravascular contribution to the measured blood flow is negligible in SPECT. Perfusion MRI, on the other hand, is based on the transient signal change caused by a contrast agent during its first pass within the blood vessels through the brain.[4,5] The diffusion of the contrast agent across the blood-brain barrier in the time frame of the data acquisition is negligible.

Perfusion MRI showed larger interindividual variability in rCBF than SPECT. Two factors may contribute to this increased variability in pMRI: 1) Statistical errors as a result of the complicated rCBF calculation and 2) variations in the vasculature among individuals. Our data suggest that the second factor, i.e., anatomic variations in the vasculature, is mostly responsible for the increased variability in pMRI. First, simply eliminating pixels with very high rCBF values significantly improved the interindividual variability of rCBF in almost all regions analyzed. Visual inspection of the signal-versus-time curves showed that such high rCBF values are associated with large signal drops during the first pass of the contrast agent, and are not caused by errors in the rCBF calculation. Second, large vessels have a prominent appearance in the rCBF maps from pMRI (Fig. 1) and may easily cause differences between SPECT and pMRI. For example, the temporal gray matter region studied included the large vessels from the branches of the middle cerebral artery, yielding high rCBF in pMRI despite moderate rCBF in SPECT (see Fig. 1). Conversely, the visual cortex shows high rCBF on SPECT but intermediate rCBF in pMRI because there were only few large vessels.

Additional differences in relative rCBF between the two methods may be explained by differences in the sensory conditions between the two scans, since activated brain regions may show increased rCBF. Although the visual conditions during the two scans were very similar (dim lighting without visually salient features), the acoustic conditions were very different. There is considerable, unavoidable, acoustic noise during the MRI scan but not during the injection of the SPECT tracer. As previous activation studies with functional MRI have demonstrated, such acoustic noise, which is essentially a monotonous tone, activates well-defined regions in the primary auditory cortex in the temporal lobes.[17] Some of these activated regions (with increased rCBF) may have been included in our temporal gray matter ROIs, possibly reducing the correlation between SPECT and pMRI.

Another factor that may reduce the correlation in rCBF between the two methods is the difference in the spatial resolution between SPECT and pMRI. Since the resolution of SPECT is much lower than that of pMRI, rCBF in the small gray matter regions analyzed, such as the deep gray matter regions, may be underestimated in SPECT due to volume averaging with the adjacent white matter which has lower rCBF than gray matter. Table 1 shows, however, that the relative rCBF in all four deep gray matter regions is higher in SPECT than in pMRI, a finding that cannot be explained by the differences in spatial resolution.

*Elimination of Large Vessels*

To attenuate the influence of large vessels on rCBF maps obtained with gradient echo techniques, we excluded all pixels from the analysis that exhibited rCBF values above a certain threshold. The choice of the threshold for ELV (2.5 times the median of all rCBF values) was validated visually. After aligning the pMRI and structural scans on a workstation, visual inspection confirms that most pixels with an rCBF above the threshold are associated with larger vessels on structural MRI. Also, the number of pixels above the threshold was relatively small, typically only 6% of the total number of pixels in the brain.

Our simple and efficient algorithm for ELV significantly reduced the variability of rCBF in most brain regions; typical relative standard deviations with ELV were below 10% in the cortex and between 10–15% in most other regions. Elimination of large vessels by postprocessing has the same goal as acquisition-based methods to attenuate the influence of large vessels in pMRI, for example, by the use of spin-echo and 'asymmetric spin-echo' EPI sequences.[18–20] While the sensitivity of gradient-echo images to intravascular gadolinium increases with the vessel diameter, spin-echo images exhibit a max-

imum sensitivity for vessel diameters of approximately 5 $\mu$m.[19] However, due to rather long acquisition times, the MRI signal of any EPI-based single-shot imaging sequence contains some contributions from gradient-echoes, and is thus influenced by larger vessels. Future studies will demonstrate whether rCBF maps obtained with spin echo techniques are superior to those obtained with pure gradient echo sequences followed by ELV.

## CONCLUSION

This paper evaluates measurements of cerebral perfusion obtained with a well-established nuclear medicine technique and a relatively new MRI technique. Over all regions, rCBF measured with these two methods correlated well after elimination of large vessels in pMRI. However, differences in the mechanisms underlying the two methods caused a lack of correlation in most individual brain regions. SPECT uses a diffusible tracer that penetrates the blood brain barrier during its first pass through the brain, while pMRI uses a purely intravascular tracer. As a result, pMRI is sensitive to the presence of large vessels, while SPECT is not. Eliminating large vessels in rCBF maps from pMRI attenuates the influence of anatomic variations in the cerebral vasculature and thus reduces interindividual standard deviations. The resulting improvement in reproducibility of pMRI should be useful for both research and clinical applications.

*Acknowledgments*—This study was supported by a fellowship from the French Foundation for Alzheimer Research, a scientist development award for Clinicians from NIDA (00280 K-20), and the UCLA Alzheimer Disease Center (AG-10123–03). We would like to thank D. Osborn, D. O'Brien, D. McGee, and C. Thomas for performing the perfusion MRI and SPECT scans, K. Hsieh for helping with the preparation of the manuscript, and Drs. M. Mehringer and F. Mishkin for their continued support of our research.

## REFERENCES

1. Powers, W.; Raichle, M. Positron emission tomography and its application to the study of cerebrovascular disease in man. Stroke 16:361–376; 1985.
2. Phelps, M.; Grubb, R.; Ter–Pogassian, M. In vivo regional cerebral blood volume by x-ray fluorescence: Validation of the method. J. Appl. Physiol. 35:741–747; 1973.
3. Kuhl, D.; Reivich, M.; Alavi, A.; Nyary, I.; Staum, M. Local cerebral blood volume determined by three-dimensional reconstruction of radionuclide scan data. Circ. Res. 36:610–619; 1975.
4. Villringer, A.; Rosen, B.R.; Belliveau, J.W. Dynamic imaging with lanthanide chelates in normal brain: Contrast due to magnetic susceptibility effects. Magn. Reson. Med. 6:164–174; 1988.
5. Rosen, B.R.; Belliveau, J.W.; Chien, D. Perfusion imaging by nuclear magnetic resonance. Magn. Res. Q. 5:263–281; 1989.
6. Edelman, R.R.; Mattle, H.P.; Atkinson, D.J.; Hill, T.; Finn, J.P.; Mayman, C.; Ronthal, M.; Hoogewoud, H.M.; Kleefield, J. Cerebral blood flow: Assessment with dynamic contrast-enhanced T2 weighted MR imaging at 1.5 T. Radiology 176:211–220; 1990.
7. Kucharczyk, J.; Mintorovitch, J.; Asgari, H.S.; Moseley, M. Diffusion/perfusion MR imaging of acute cerebral ischemia. Magn. Reson. Med. 19:311–315; 1991.
8. Harris, G.; Lewis, R.; Satlin, A.; English, C.; Scott, T.; Yurgelun–Todd, D.; Renshaw, P. Dynamic Susceptibility Contrast MRI of Regional Cerebral Blood Volume in Alzheimer's Disease. Am. J. Psychiatry 153:721–724; 1996.
9. Johnson, K.; Renshaw, P.; Becker, J.; Satlin, A.; Holman, B. Comparison of Functional MRI and SPECT in Alzheimer's Disease. Neurology 45:A405–A406; 1995.
10. Moseley, M.; de Crespigny, A.; Roberts, T.; Kozniewska, E.; Kucharczyk, J. Early detection of regional cerebral ischemia using high-speed MRI. Stroke 24:I60–I65; 1993.
11. Renshaw, P. F.; Levin, J. M.; Kaufman, M. J.; Ross, M. H.; Lewis, R. F.; Harris, G. J. Dynamic susceptibility contrast magnetic resonance imaging in neuropsychiatry: Present utility and future promise. Eur. Radiol. 7:216–221; 1997.
12. Fisel, C.; Ackerman, J.; Buxton, R.; Garrido, L.; Belliveau, J.; Rosen, B.; Brady, T. MR contrast due to microscopically heterogeneous magnetic susceptibility: Numerical simulations and applications to cerebral physiology. Magn. Reson. Med. 17:336–347; 1991.
13. Bahn, M.M. A single-step method for estimation of local cerebral blood volume from susceptibility contrast MRI images. Magn. Reson. Med. 33:309–317; 1995.
14. Neirinckx, R.D.; Canning, L.R.; Piper, I.M.; Nowotnick, D.P.; Pickett, R.D.; Holmes, R.A.; Volkert, W.A.; Forster, A.M.; Weisner, P.S.; Marriott, J.A.; Chaplin, B.S. Technetium-99 m d,l-HMPAO: A new radiopharmaceutical for SPECT imaging of regional cerebral blood perfusion. J. Nucl. Med. 28:191–202; 1987.
15. Itti, L.; Chang, L.; Ernst, T.; Mishkin, F. Improved 3-D correction for partial volume effects in brain SPECT. Human Brain Mapping 5:379–388; 1997.
16. Itti, L.; Chang, L.; Mangin, J.F.; Darcourt, J.; Ernst, T. Robust multimodality registration for brain mapping. Human Brain Mapping. 5:3–17; 1997.
17. Bandettini, P. A.; Jesmanowicz, A.; Van Kylen, J.; Birn, R. M.; Hyde, J.S. Functional MRI of brain activation induced by scanner acoustic noise. Magn. Reson. Med. 39:410–416; 1998.
18. Kwong, K.; Chesler, D.; Zuo, C.; Boxerman, J.; Baker, J.; Chen, Y.; Stern, C.; Weisskoff, R.; Rosen, B. Spin echo ($T_2$, $T_1$) studies for functional MRI. In: Book of abstracts: Society of Magnetic Resonance in Medicine. New York, NY: SMRM, 1993: p. 172.
19. Boxerman, J.; Hamberg, L.; Rosen, B.; Weisskoff, R. MR Contrast due to intravascular magnetic susceptibility perturbations. Magn. Reson. Med. 34:555–566; 1995.
20. Bandettini, P.A.; Wong, E.C.; Jesmanowicz, A.; Hinks, R. S.; Hyde, J.S. Spin-Echo and Gradient-Echo EPI of human brain activation using BOLD contrast: A comparative study at 1.5T. NMR Biomed. 7:12–20; 1994.